ESOMAT 2009, 08001 (2009)
DOI:10.1051/esomat/200908001

Roundrobin SMA modeling

P.Sittner[1,a], L.Heller[1], J. Pilch[1], P.Sedlak[2], M. Frost[2], Y. Chemisky[3], A. Duval[4] , B.Piotrowski[4], T. Ben Zineb[4], E. Patoor[3], F. Auricchio[5] , S. Morganti[5], A. Reali[5], G. Rio[6] , D. Favier[7] , Y. Liu[8], E. Gibeau[9], C. Lexcellent[9] , L. Boubakar[9] D. Hartl[10], S. Oehler[10], D.C. Lagoudas[10] and Jan Van Humbeeck[11]

[1]Institute of Physics Academy of Sciences of the Czech Republic, Prague, 18221 Czech Republic
[2]Institute of Thermomechanics Academy of Sciences of the Czech Republic Prague, 18221 Czech Republic
[3]LPMM, Metz University, Arts et Metiers ParisTech, CNRS, Ile du Saulcy 57045 Metz, France
[4]LEMTA , Nancy University, CNRS, 2 rue Jean Lamour, 54500 Vandoeuvre-les-Nancy, France
[5]Dipartimento di Meccanica Strutturale (DMS), Universit` degli Studi di Pavia, Via Ferrata 1, 27100 Pavia, Italy
[6]Université Européenne de Bretagne, LIMATB, Rue de Saint Maudé - BP 92116, 56321 Lorient cedex, France
[7]Université de Grenoble/CNRS, 3S-R, BP 53, 38041 Grenoble Cedex 09, France
[8]The University of Western Australia. School of Mechanical Engineering, Crawley, WA 6009, Australia
[9]FEMTO-St Département de Mécanique Appliquée, 24 rue de L'Epitaphe 25000 Besançon France
[10]Department of Aerospace Engineering, Texas A&M University, College Station, TX, USA
[11]MTM Departement KU Leuven Belgium

Abstract. This article reports on an ESF S3T EUROCORES sponsored networking activity called Roundrobin SMA modeling organized with the aim to compare capabilities of various thermomechanical models of shape memory alloys capable to simulate their functional responses for applications in smart engineering structures. Five sets of experimental data were measured in thermomechanical tests on thin NiTi filament in tension, torsion and combined tension/torsion. The data were provided to six teams developing advanced SMA models to perform appropriate simulations. Simulation results obtained by individual teams were compared with experimental results and presented on a dedicated Roundrobin SMA modeling website. The evaluation of the activity in terms of the assessment of the capability of individual models to deal with specific features of the experimentally measured SMA thermomechanical responses is provided in this article.

1 Introduction

Shape memory alloys (SMA) show highly nonlinear hysteretic stress-strain-temperature thermomechanical behavior due to martensitic phase transformations reversible up to about 5% tensile strain while reaching stresses of about 1GPa in thousands of cycles. This yields very large mechanical energy which can be utilized in smart structures for actuation, damping, impact absorption or simply as a material for highly elastic (superelastic) parts of engineering structures [1]. SMAs have been around for over the last five decades and many mechanics models capable of simulation of their thermomechanical responses (SMA models) have been developed and published in the literature since then (see section 3 and references [14-37] discussed there). Nevertheless, when one tries to use these models to design or safely control smart engineering structures, serious problems frequently arise. The problems seriously limit wider applicability of SMA materials. While trying to identify the reasons and to find best solutions for these problems within the community of European researchers involved in the smart structure design and control [2], it turned to be very difficult to achieve mutual agreement between individual teams developing rather different SMA models.

Following issues were identified as main sources of problems:

1. Functional responses of SMA elements are thermomechanical hysteretic in nature, which requires the SMA models to predict great variety of stress-strain-temperature responses with single set of material parameters. There is no agreement on selection of material parameters and method to extract them.
2. Multiple very different deformation mechanisms proceed in a thermomechanically loaded SMA element depending on stress, strain and temperature conditions.

[a] e-mail: sittner@fzu.cz

Article available at http://www.esomat.org ou http://dx.doi.org/10.1051/esomat/200908001

3. SMA models must be able to capture partial (internal) cycle responses of SMA elements in thermal, mechanical or thermomechanical loads.
4. Mechanical responses of SMA elements in which strain gradients are present remain to be a problem.
5. There is still a lack of good experimental data for general multiaxial loading conditions, particularly for non-proportional loading.

As a way out of the discussions, it was decided to perform an activity called "Roundrobin SMA modeling" - a kind of benchmark for SMA models available within the S3T community which would test their ability to deal with the five key issues listed above. Later on, three additional well known research teams joined the activity forming a group of six teams (Table 1), the representatives of which are listed as authors of this article. The same sets of experimental data were given to all participating teams to perform appropriate simulations and the simulation results were compared with experiments. Detailed information about the activity including history of events, complete experimental datasets, all individual modeling articles [5-10] and evaluation of the activity can be found on a Roundrobin SMA modeling website [3] built to disseminate the results.

Selection of the particular experimental tests to be simulated was inspired by the 5 key issues listed above. A thin superelastic medical grade NiTi wire NiTi#1 [4] delivered by Fort Wayne Metals was selected as an SMA element to be used in the benchmark experiments. Deformation behavior of the wire was studied in simple thermomechanical tests in tension, torsion and combined tension/torsion (5 datasets described in section 2). An introduction to the SMA modeling is presented in section 3. Description of SMA models used in the Roundrobin and simulation results achieved by individual modellers are presented in articles [5-10] written by individual teams and their complete set can be found on the Roundrobin website [3]. Section 4 contains an evaluation of the benchmark based on the comparison of simulation and experimental results. Since the main goal of the activity was to map how individual rather different SMA models approach the problem, we have mainly tried to identify the experimental features posing problems in simulations, asses their treatment by individual models and find out the consequences of these treatments for the quality of simulations.

TABLE 1: Roundrobin SMA modeling: teams and models

Model shortcut [Ref]	**Authors**	**Model description**	**No. of independent material parameters**
Fro [5]	P.Sedlak, M. Frost, P.Sittner	FEM implemented SMA hysteretic algorithm for multiple deformation processes in NiTi	32
Che [6]	Y. Chemisky, A. Duval, B.Piotrowski, T. Ben Zineb, E. Patoor	FEM implemented 3D thermodynamics based model with 3 internal variables	16
Rea [7]	F. Auricchio , S. Morganti, A. Reali	FEM implemented 3D constitutive SMA model	7
Gib [8]	E. Gibeau, C. Lexcellent, L. Boubakar	FEM implemented 3D thermodynamics model based on transformation surface of SMA	24
Rio [9]	G. Rio, D. Favier, Y. Liu	FEM implemented 3D thermomechanics model based on discrete memory elastohysteresis theory	21
Har [10]	D. Hartl, S. Oehler, D.C. Lagoudas	FEM implemented 3D thermodynamics model	15

2 Experimental Datasets

SMA models are commonly used for three typical purposes in smart structure research: i) to design SMA elements of complicated shape (e.g. medical stent design), ii) to simulate forces and elongations encountered in SMA actuator applications (e.g. design of SMA spring actuator) and iii) to perform active control of smart structures with SMA elements (e.g. active control of deflection of SMA polymer composite beam). Each of these applications is sensitive to different aspects of SMA modeling. While complex SMA elements in smart structures (i) are designed with FEM implemented SMA models capable of simulating general multiaxial loads with strain gradients, the actuator and control applications demand mainly the ability of SMA models to simulate partial thermomechanical cycles in wide temperature and stress ranges. This was mainly kept in mind when selecting the experimental datasets for the Roundrobin SMA modeling benchmark.

2.1 Superelastic NiTi wire as SMA element

There are two major problems appearing when confronting simulation and experimental results of SMA thermomechanical behaviors. The first is the instability of cyclic thermomechanical responses due to irreversible plastic deformation accompanying the recoverable deformation due to martensitic transformation. In case of NiTi, the resistance against dislocation slip depends heavily on the microstructure [11]. In order to minimize the cyclic deformation instability, high strength (1.6 GPa) superelastic medical grade NiTi wire (straight annealed NiTi#1) of the thickness 0.01mm was selected as the SMA element for the benchmark. These wires, following a training for particular applied loading mode (e.g. 100 cyclic tensile tests beyond the end of plateau at room temperature) show very stable cyclic response. The training thus allows for performing multiple tests on a single sample.

Second there is a problem with strain localization in NiTi wire loaded in tension. It obviously affects the experimental results but it is not considered in SMA modeling dealing with homogeneous deformation. The possibility to avoid either NiTi (use other SMA) or tension (use e.g. compression) was excluded due to the reason that the NiTi wire loaded in tension is the most common material and geometry used in SMA research. Therefore, it is not expected that the simulation will reproduce sharp yield points or flat stress plateaus in tensile tests at constant temperature which are clearly due to the localized deformation mode. On the other hand, plateau stress level, length of the transformation plateau or hysteresis width are expected to be reproduced in simulations although the confrontation with experiments is due to the strain localization in tension questionable. Basic material parameters characterizing the NiTi wire evaluated by IP ASCR team are presented in Table 2. More information concerning the parameters and evaluation methods can be found on the Roundrobin website [3].

TABLE 2: Basic material parameters characterizing the NiTi wire

Material parameter	**value**
R-phase start temperature	25 ^{o}C
R-phase finish temperature	5 ^{o}C
Young modulus of austenite	53.6 GPa
Young modulus of martensite	21.1 GPa
Transformation Yield stress of austenite at room temperature	555 MPa
Maximum recoverable transformation strain	5.2%
Ultimate tensile strength	1590 MPa
Yield stress	1330 MPa
Strain at failure	13 %
Pseudoelastic stress hysteresis	336 MPa
Accumulated nonrecovered strain for N=100	0.47 %
Cyclic accumulated transformation stress change for N=100	24.5 %
Cyclic accumulated pseudoelastic hysteresis change for N=100	24 %
Effective martensite start temperature	-72 ^{o}C
Effective austenite finish temperature	-0.4 ^{o}C
Temperature dependence of transformation stress for A-R	15.9 MPa/^{o}C
Temperature dependence of transformation stress for A-M	5.57 MPa/^{o}C

2.2 Testing equipment and methods

Experimental tests were performed on three testing machines optimized for thermomechanical testing of thin NiTi filaments for application in smart textiles. All testing machines are equipped with electrically isolated grips, Peltier furnaces and systems for in-situ measurement of electrical resistance of the wire. Evaluation of electrical resistance of the wire during the tensile tests is beneficially used to draw information on the deformation mechanism involved (B2-R, B2-B19', martensite reorientation) [12].

Figure 1 shows a unique purposely made equipment used to perform combined tension/torsion tests on thin NiTi filaments called ATTUT. The device consists of stepping motor to apply torque on the sample, a linear inductive transducer to measure axial elongation of the sample, axial dead load to apply tension to the sample, an electrical resistance measurement circuit and Peltier furnace to control temperature of the sample. The torque of the thin NiTi wire is very small for conventional torque cells. Instead of a torque cell the system contains a comparator device consisting of a tungsten wire and NiTi wire connected with stainless steel tube in series. Separate measurements of the angular displacement of the thin NiTi filament φ_2 and the tungsten wire φ_1 are made with a rotary code wheel. The torque is calculated using equation 1.

$$M_k = -\frac{\pi \cdot G_{TW} \cdot {d_{TW}}^4 \cdot (\varphi_1 - \varphi_2)}{32 \cdot l_{TW}} \tag{1}$$

l_{TW} , d_{TW} and G_{TW} are parameters of the tungsten wire length, diameter and shear modulus, respectively. Combined tension-torsion thermomechanical tests were run with automated control LabVIEW program. A basic test includes either at constant temperature varying the angular displacement either at constant angular displacement varying the temperature.

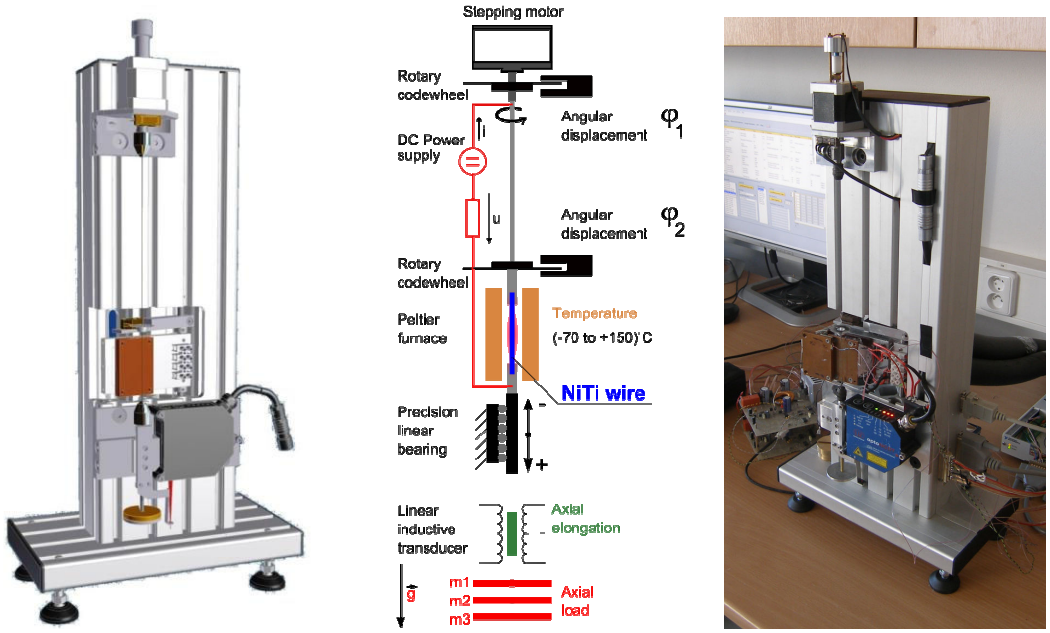

Figure 1: Combined tension-torsion tester ATTUT designed and built at IP ASCR to evaluate functional properties of thin metallic filaments

Only one NiTi wire sample was used in experiments performed to obtain experimental data. The wire was first trained by 100 cycles to stabilize its mechanical response for particular type of loading (tension, torsion). In case of combined tension-torsion (dataset 4), a new sample trained by 10 tensile cycles at 50 ˚C was used in each test. Hereupon series of tests corresponding to 5 different datasets (section 2.3) have been performed. Out of these series, selected experimental responses (Figs 2-6) were selected for simulation benchmark.

Before each test, the sample was heated in stress free state well above A_f temperature (T=395K) and cooled down to test temperature to minimize the effect of the history on the stress-strain response. All tests were performed in position (torsion angle) control mode, in combined tension–torsion test (dataset 4) a constant tensile force was applied. The test temperature was controlled by a Peltier furnace in all tests. This is essential since any change of environmental temperature or heat transfer conditions at the thin wire surface have dramatic impact on the recorded stresses and strains. The tests were performed at low strain rates ($<10^{-3}$ s^{-1}) in order to minimize the selfheating effects [13] on the recorded stress-strain responses. All tests in which temperature was varied in time (datasets 2 and 5) were performed at low temperature rates (<10˚C/min) to assure well defined test conditions.

2.3 Selection of thermomechanical tests

The following five sets of experimental data obtained from different tests on the same SMA element (NiTi #1 superelastic wire) were selected for the simulation benchmark.

1. **Tensile stress-strain tests** at three constant temperatures T = -20 ˚C, T = 10 ˚C and T = 60 ˚C (Fig. 2).
2. **Thermal cycling tests at constant applied tensile stress** – Strain-temperature curves recorded in thermal cycle through the transformation interval under three different constant tensile stresses 300 MPa, 400 MPa and 500 MPa (Fig. 3).
3. **Torsion symmetrical tests** - Torque-torsion angle symmetrical +/- responses at constant tensile stress 70 MPa and three constant temperatures - T = -30 ˚C, T = -10 ˚C and T = 30 ˚C (Fig. 4).
4. **Combined tension-torsion tests** - Torque-torsion angle symmetrical +/- responses at temperature T = 30˚C and four constant axial stresses 70 MPa, 255 MPa, 317 MPa, 379 MPa (Fig. 5).
5. **Thermomechanical recovery stress tests** – Stress-strain and stress-temperature curves recorded in thermomechanical tests involving tensile deformation at room temperature T = 26 ˚C (>A_f) up to 3.5 % prestrain (both at upper and lower plateau), followed by thermal cycling at constant prestrain and final unloading at room temperature (Fig. 6).

The datasets 1 and 2 were included as basic tests which are most frequently performed on SMA elements in the literature. Uniaxial homogeneous tensile stress and strain are expected to exist everywhere in the wire. The results of these tests (Figs. 2 and 3) were used by some modelers to obtain some of the material parameters possibly different from those presented in Table 2.

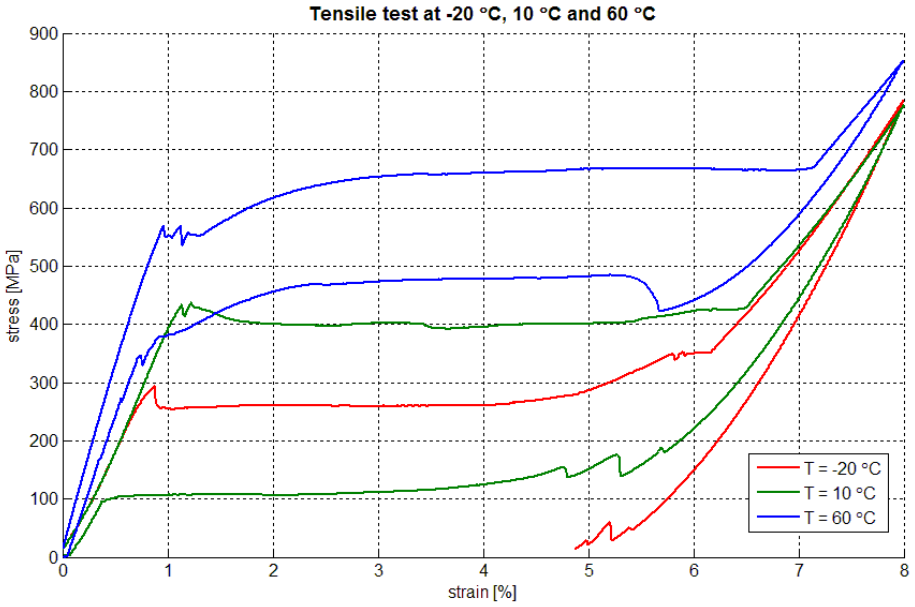

Figure 2: Tensile stress-strain curves at three constant temperatures T = -20 ˚C, T = 10 ˚C and T = 60 ˚C.

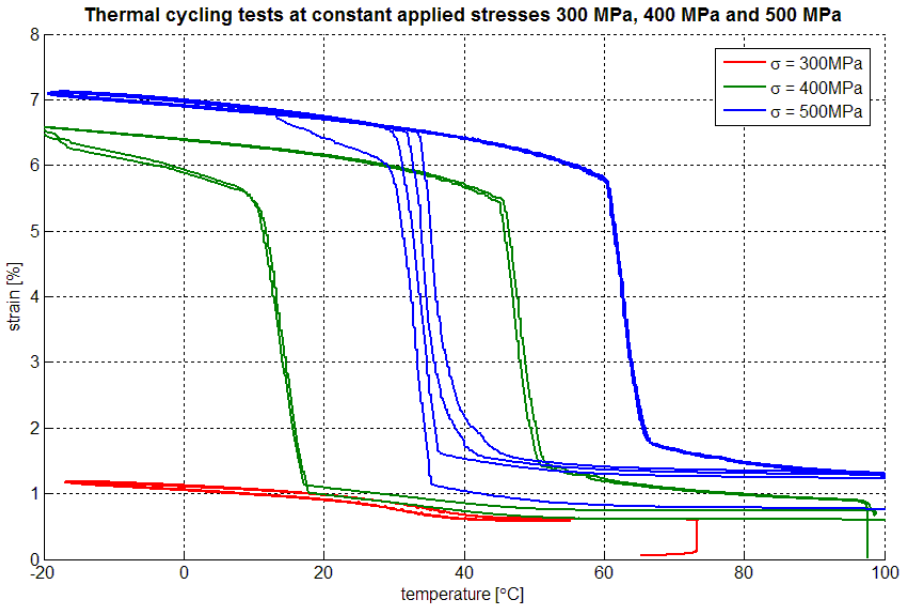

Figure 3: Strain-temperature curves recorded in thermal cycle through transformation interval under three different tensile constant stresses 300 MPa, 400 MPa and 500 MPa.

The symmetrical torsion test (dataset 3, figure 4) was included to test the ability of the models to simulate the responses of elements where strain gradient exists as well as to capture the behavior of the SMA element exposed to loads in which deformation in martensite may become prevailing deformation mechanism (reloading in torsion+/-).

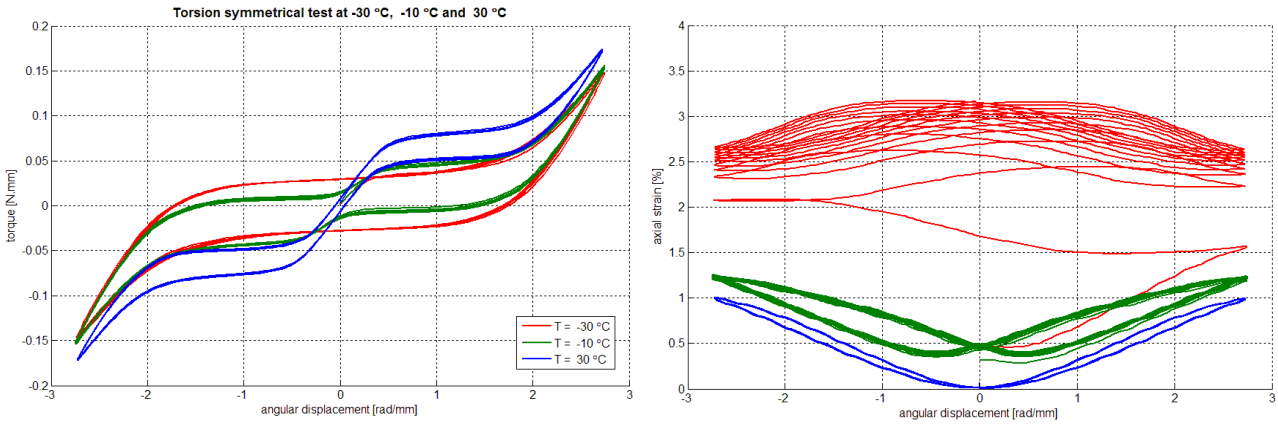

Figure 4: Torque-torsion angle and axial strain –torsion angle responses at constant tensile stress 70 MPa and three constant temperatures - T = -30 ˚C, T = -10 ˚C and T = 30 ˚C.

Combined tension-torsion tests (dataset 4, figure 5) provide experimental data for general nonproportional loading behavior of the SMA element.

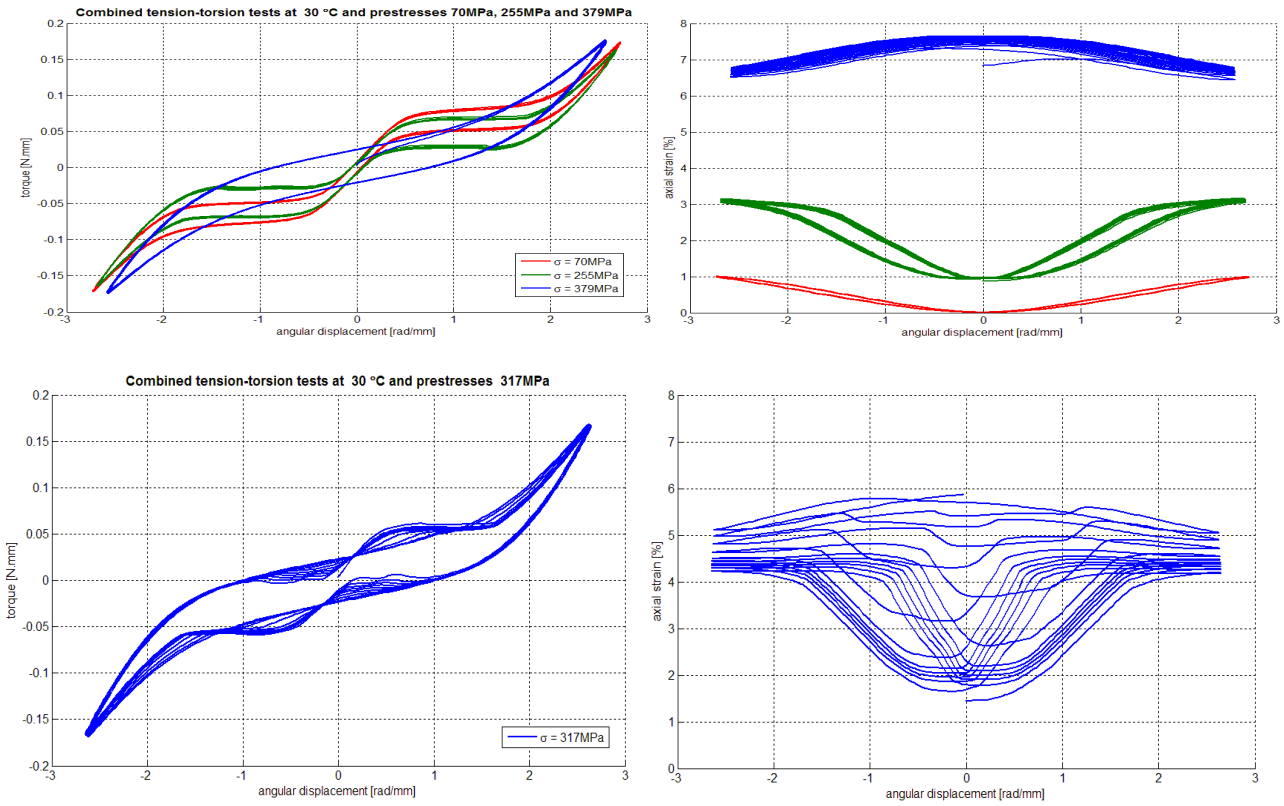

Figure 5: Torque-torsion angle and axial strain–torsion angle responses at constant temperature T = 26 ˚C and four constant axial stresses 70 MPa, 255 MPa, 317 MPa, 379 MPa.

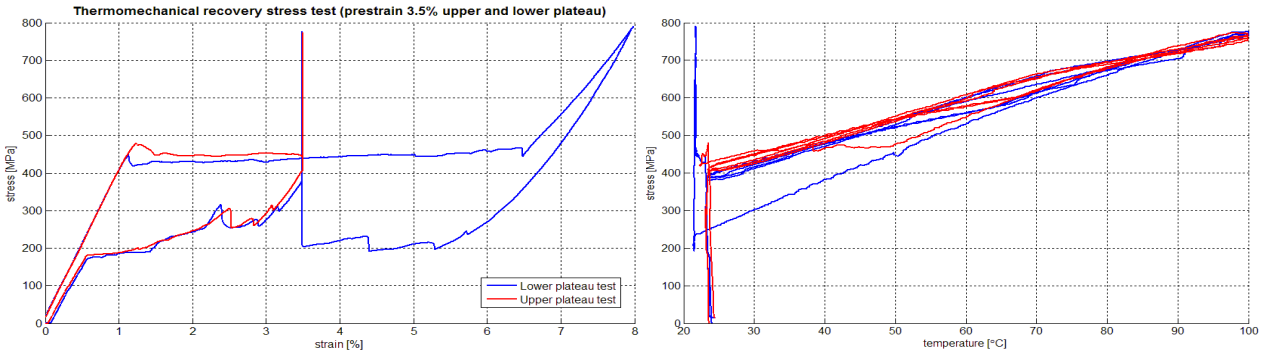

Figure 6: Stress-strain and stress-temperature curves recorded in thermomechanical recovery stress tests involving tensile deformation at room temperature T = 26 ˚C up to 3.5 % prestrain, followed by thermal cycling at constant prestrain and final unloading at room temperature.

Finally, the recovery stress tests (dataset 5, figure 6) concern general thermomechanical loadings in which history dependence and partial cycle responses become very important and challenging for simulations.

3 SMA models

SMA models applicable for simulation of adaptive structures with SMA elements can be roughly divided between microscopic models (internal variables are defined at the grain scale, [14-19]) and macroscopic models (internal variables are defined at the representative volume element /RVE/, [20-33]).

The microscopic models are based on the description of the martensitic transformation effect at the grain scale. Each martensite variant is characterized by a habit plane, a twinning direction (material parameters) and a volume fraction (internal variable). A free energy expression is defined by considering mechanical, chemical, interface and interaction energies. The driving force associated to each volume fraction is derived from the free energy expression and is compared to the critical one in order to manage the activation process. Finally the consistency rule is adopted and the local constitutive model is derived. A scale transition homogenization technique (self consistent [17], Taylor [18]…) is adopted for the determination of the effective macroscopic behaviour of a RVE composed of a representative aggregate with a given crystallographic texture. These kinds of models present an accurate and physical description of the SMA thermomechanical behaviour. However, they have a large number of internal variables which makes their implementation in a finite element codes complicated. Therefore, they are used only exceptionally in smart structure design or control. Nevertheless, they remain very useful for optimization of material performance and/or eventually to identify parameters of macroscopic models.

The macroscopic models are derived from thermodynamical approach, [20,22-25,27,31] or plasticity and viscoplasticity theories, [21,26,28-30,32-33]. In the first case, a thermodynamical potential expression is assumed or derived from micromechanical considerations. Generally the free energy of Gibbs or Helmoltz is considered as a potential function of macroscopic control and internal variables and material parameters. As for the micromechanical models, the driving forces associated to internal variables are derived from such potential and are compared to the critical ones in order to manage the activation of various inelastic processes (phase transformation, martensite reorientation). The consistency rule and the normality one or a dissipation potential are assumed leading to non linear constitutive equations. In the plasticity-inspired models, the inelastic strain induced by phase transformation is assumed to be similar to one corresponding to plastic gliding. In that case an analogy is assumed with the theory of plasticity by introducing a transformation surface which can be expanded as for an isotropic or/and kinematic hardening. The constitutive equations are derived in the same way as in plasticity. This set of models describes very well the superelastic behavior due to stress induced martensitic transformation. The martensitic transformation strain is assumed to be oriented by the deviatoric part of the stress tensor. An extension to the case of martensite reorientation is proposed, for example in [30, 33, 34]. Other macroscopic models are also proposed by interpolating the behaviour surface in a 3D stress – strain – temperature by various classical functions [32].

Most of these models adopt a classical decomposition of the total strain in an elastic part and an inelastic one. The effects of martensitic phase transformation and martensite variants reorientation are gathered in the inelastic

strain expression. However, few models adopt the decomposition of the stress tensor in a reversible part and a hysteretic one [29]. The reversible stress is derived from a hyperelastic theory by assuming an expression of the density energy. The hysteresis stress is irreversible and its expression is derived from rheological models containing elastic and slip elements. This leads to a general pure hysteresis model involving the notion of discrete memory. In the case of macroscopic models with strain decomposition, the inelastic strain is defined with a set of scalar (volume fraction of total, stress induced or oriented and self accommodated or thermal martensite), and tensorial internal variables (mean transformation strain, mean twinning strain in martensite). Some models consider the rate of change of oriented and self accommodated martensite volume fraction [28].

All SMA models consider some additional relations in order to take into account various specificities of SMA behaviour. The saturation effect is taken into account by introducing saturated functions in the kinetic laws, or Lagrangian multipliers or penalization functions in the thermodynamic potential. The hysteretic effect is taken into account by considering different values of critical forces during loading and unloading. Finally the internal loop behavior is described by various techniques as for example assuming a critical force depending on the last value of martensite volume fraction before unloading. Most of the macroscopic models are implemented in finite element codes and used for SMA structural analysis. Many extensions of these models are under continuous development, for example in order to take into account the effect of precipitates or the interaction between transformation and plasticity or viscoplasticity during monotonic or cyclic loading [35-37].

4 Evaluation

In this section we shall discuss SMA modeling approaches (section 3) represented by Roundrobin teams (Table 1) based on the comparison of simulation results with experimental data (section 2). Complete presentation of simulation results can be found on the Roundrobin SMA modeling website [3]. A brief presentation of SMA models including selected simulation results can be found in individual modeling articles [5-10].

4.1 Uniaxial thermomechanical tests in tension

The experimental results in datasets 1 and 2 present examples of basic uniaxial tests in which the martensitic transformation is driven by increasing stress or temperature and homogeneous stress and strain distribution is assumed to exist. In fact this is not true for the tensile test on NiTi wire at constant temperature where localization of deformation in shear bands typically occurs as discussed in section 2.1. In spite of this, practically all models predict quite well the experimental results, particularly the stress-temperature conditions at which cubic to monoclinic transformation takes place, hysteresis width and transformation strain.

The differences between simulations and experimental results are, however, in details. For example, the B2-R transformation which occurs around room temperature is a problem for all models. It causes lowering of the apparent elastic modulus of austenite in tensile test below 30°C (Fig. 2). R-phase is also responsible for small inelastic reversible strains observed in thermal cycles at low applied stress (Fig. 3). Note that, except for the model Che, all models show transformation strains due to cubic-monoclinic phase transformation during thermal cycling at 300MPa, where the experiment exhibits only strains due to B2-R transformation. The model treats this correctly due to the adopted nonlinear forward transformation condition (Fig. 1 in ref [6]). Similar problems appear in modeling treatment of highly nonlinear response in martensite state beyond the end of the plateau (Fig. 1). The models which determine the material parameters from experimental curves (Fro, Rio) and allow for simulation of nonlinear nonhysteretic response show best agreement with experiments, particularly as regards the elastic ranges prior and after the stress plateau. Another feature is the decrease of the stress (temperature) hysteresis width with increasing temperature (stress) in tensile tests (thermal cycling at constant stress). Only some of the continuum thermodynamics based models (Che, Gib, Har) seem to capture this.

4.2 Symmetrical torsion test

The symmetrical torsion tests at three different temperatures in dataset 3 (Fig. 4) involve either stress induced transformation (T = 30 ˚C) or deformation in martensite (T = -30 ˚C) or mixture of both deformation mechanisms (T = -10 ˚C). Since there is a strain gradient from the wire surface to the core, all models use some kind of FEM implementation to simulate the responses. All models capture reasonably well the experimental curves, the models Fro and Rea show best agreement. All true 3D models (Che, Rea, Har, Gib) tend to overestimate the length of the plateau in angular displacements in torsion. This is most likely due to the very strong texture in the thin wire which affects the transformation surface [38] which is not taken into account in isotropic models. The asymmetry in tension/compression, which is accounted for in all models, originates from the transformation anisotropy associated with the cubic to monoclinic martensitic transformation in NiTi [40].

The models nevertheless remain isotropic and hence the tension / compression asymmetry does not solve the problem of the length of the plateau in angular displacements in torsion.

All models capture the torsion responses at the lowest temperature (deformation in martensite) and at the highest temperature (stress induced transformation) quite well. Except of Rea, all models also seem to simulate well also the increase of the hysteresis width with decreasing temperature successfully. This is probably related to the way how martensite reorientation is implemented and parameterized.

The torsion test at intermediate temperature T = -10˚C is characterized by S-shaped two plateau hysteretic torque – angular displacement curves. This temperature was selected intentionally since it was expected that above this temperature stress induced transformation operates as deformation mechanism while below this temperature martensite reorientation may take place during cycling. If both deformation mechanisms operate, simulation results are very sensitive to their implementation and parameterization. One can see that the minimum of axial strain becomes shifted from 0 angular displacement position to the two minima with temperature decreasing from 30°C to -10°C but the response is still stable. This is due to the fact that the strains due to stress induced transformation are not completely recovered upon torsion unloading. They can be recovered by reverse martensitic transformation (-10^{o}C). Only Fro and Rea models seem to capture this properly. Or alternatively they can be recovered by martensite reorientation (-30^{o}C) driven by opposite torsion- loading. In that case deformation mechanism changes from stress induced transformation to martensite reorientation. In the test at T=-30^{o}C an unusual instability of the mechanical response of the wire is observed during first few cycles (Fig. 4, T=-30^{o}C). This ratcheting has nothing to do with dislocation plasticity, all strains are fully recoverable upon heating since they are solely due to phase transformation. Among the Roundrobin models, only model Che seems to capture this ratcheting at least qualitatively. In modeling, the ratcheting is related to the interaction between the various elements with very different stress levels in the FEM implementation of the torsion problem. In this respect, it would be very interesting to know the gradients of strain, stress and martensite phase fraction from the surface to the core of the wire which is available in all simulations. Information on martensite fraction gradient in torsion test can be found in figure 4 in ref. [6]. In the torsion test at lowest temperature T=-30 ^{o}C, the deformation mechanism changes from stress induced transformation to stable response due to martensite reorientation following the first symmetrical torsion cycle. All models seem to capture this.

4.3 Combined tension-torsion test

Combined tension-torsion experiments (dataset 4) were intended to test the implementation of the general nonproportional loading behavior of the SMA element in the SMA models. Main feature to be followed is the coupling between tension and torsion (the reversible axial strain developing upon torsional loading (Fig. 5)) which is very different in superelastic range (axial stresses 70-255 MPa) and reorientation range (379 MPa). All models seem to capture the consequences of this coupling surprisingly well, although some models underestimate (Fro) and some overestimate (Che) the axial strain response. At highest axial stress 379 MPa, where the underlying deformation mechanism is martensite reorientation only, all models except of Fro fail to simulate correctly the axial strain response probably since the stress induced transformation is still activated in the simulation. The most complicated situation occurs in the test at 317 MPa axial stress applied. In this case, stress induced transformation which is the initial deformation mechanism changes subsequently into martensite reorientation during cycling. This results in the unusual ratcheting even at room temperature. No model captures this even qualitatively, except for model Che.

4.4 Recovery stress test

The recovery stress tests (dataset 5) concern general thermomechanical loadings where mechanical and thermal loads are combined (Fig. 6). In fact, this is rather important and simulates very frequent situations, since it exists in all practical actuator, stress generation and shape memory applications of NiTi wires. The recovery stress test involves a change from stress driven to thermally driven phase transformation. In such tests, partial cycle responses and history dependences due to microstructure formation become very important and challenging for simulations. All models simulate surprisingly well the actually achieved magnitude of the recovery stress at maximum temperature T=100^{o}C as well as the stable stress-temperature responses upon heating-cooling surprisingly well. SMA models with built in hysteresis generation algorithms (e.g. Fro, Rio) show best agreement with experiments since they are best performing regarding the simulation of internal hysteretic loops. Most of the models have difficulties to simulate the difference between the stress-temperature response in the first and second heating, which is typically observed in all experiments. This is most likely due to the path and history dependence. The microstructures in the wire after superelastic loading and after first cooling (same stress, strain and temperature) are completely different (see Fig. 8d in Ref [39]). Simulations by model Che shows best agreement with experiment in this respect. Rea model predicts unrealistic wide stress-temperature hysteresis.

5 Conclusions

SMA model benchmark called Roundrobin SMA modeling was organized to mutually compare simulation results achieved by several thermomechanical models of shape memory alloys. 5 sets of experimental data obtained from thermomechanical tests on thin NiTi filament in tension, torsion and combined tension/torsion were provided to 6 teams developing advanced SMA models in Europe and US to perform appropriate simulations. Simulation results are partially reported in closely related articles [5-10] written by individual teams and confrontation of simulation vs. experimental results can be found on dedicated Roundrobin SMA modeling website [3].Following conclusions were drawn from the benchmark:

- All involved SMA models reliably predict a variety of uniaxial stress-strain-temperature responses to varying external stress (strain) and temperature conditions, particularly when stress induced martensitic transformation is involved as the dominating deformation mechanism. This is the case for the superelastic wire deformed in tension (datasets 1, 2, 5). It is vital to verify the modelling results by confronting simulation and experimental data from multiple thermomechanical tests in wide temperature range using a single set of material parameters. In this respect, simulations performed with rather different Roundrobin models show very good agreement with experiment.

- In order to simulate properly the recovery stress tests or thermomechanical actuator tests, SMA models must be able to capture correctly the shapes of partial (internal) cycle responses of SMA elements in thermal, mechanical and thermomechanical loads and related path and history dependent behaviors. SMA models with built in hysteresis generation algorithms (e.g. Fro, Rio) show best agreement with experiments and best applicability in this respect (dataset 5). These models, however, tend to use large number of independent material parameters and are less reliable regarding the treatment of multiaxial loads in wide temperature range.

- Major difficulties in formulation of appropriate constitutive equation and parameterization of SMA models stem from the activity of multiple deformation mechanisms (e.g. elasticity, B2-R transformation, B2-B19' transformation, martensite reorientation in NiTi) activated during thermomechanical loads depending on the stress, strain and temperature conditions. Models which do treat the responses due to these multiple mechanisms (at least martensitic transformation and martensite reorientation) with large number of material parameters show generally best performance (e.g. Che, Har, Fro, Gib). It is interesting to note that the Rea model achieves comparable results with 7 material parameters only.

- All models simulate the torque-angular displacement curves from symmetrical torsion tests at high temperatures (dataset 3) reasonably well. 3D models (all models except of Fro which is a 2D model) tend to overestimate the length of the plateau in angular displacements in torsion. It has been attributed to the very strong texture in the thin wire neglected in isotropic models. At lowest temperatures, the experiments show a subsequent change of the wire response in several torsion cycles – a kind of ratcheting particularly visible in axial strain – torsion angle response. It has been attributed to the subsequent switching between phase transformation and martensite reorientation deformation mechanisms. In simulations, this switching should occur subsequently in various elements used in the FEM implementation of the torsion problem. Out of the six Roundrobin models, however, only model Che seems to capture this ratcheting at least qualitatively.

- The models which account for the difference between the phase transformation and martensite reorientation deformation mechanisms (all models except of Rio) qualitatively simulate the difference between the stable superelastic responses at lowest tensile stress and stable pseudoplastic responses at highest tensile stress in combined tension-torsion tests (dataset 4). Although some models underestimate (Fro) and some overestimate (Che) the axial strain response during torsion loading of the wire this is considered to be an important success of modelling. On the other hand, it is to be noted that the above mentioned switching of deformation mechanisms during cycling (ratcheting) occurs under multiaxial loading conditions in a much wider temperature range. The consequent instability of the deformation response thus extends to higher temperatures under nonproportional multiaxial loading conditions. In particular, although this instability clearly dominates the thermomechanical behavior of the superelastic wire at room temperature (T=26^{o}C), all models fail to capture it. It has been concluded that this phenomenon is significant and more attention shall be given to it both in experiments and modelling.

Acknowledgement

This work has been supported by the European Science Foundation through the EUROCORES S3T projects MAFESMA and SMARTeR. The organizers also acknowledge support from Czech national research projects GACR P108/10/1296, P107/10/0824, AV0Z10100520, IAA200100627.

References

[1] Shape Memory Alloys Modeling and Engineering Applications, Springer, (2008), Ed. D.C. Lagoudas
[2] S3T ESF EUROCORES collaboration projects MAFESMA and SMARTer, 2008-10 http://www.esf.org/activities/eurocores/running-programmes/s3t.html
[3] http://department.fzu.cz/ofm/roundrobin
[4] http://www.fwmetals.com/nitinol-wire.php
[5] M. Frost and P. Sedlak, Roundrobin SMA modeling article, in this volume (2010)
[6] Y. Chemisky, A. Duval , B. Piotrowski, T. Ben Zineb, and E. Patoor, Roundrobin SMA modeling article, in this volume, (2010)
[7] F. Auricchio , S. Morganti, A. Reali, Roundrobin SMA modeling article, in this volume, (2010)
[8] E. Gibeau, C. Lexcellent, L. Boubakar, Roundrobin SMA modeling article, in this volume, (2010)
[9] G. Rio, D. Favier, Y. Liu, Roundrobin SMA modeling article, in this volume, (2010)
[10] D. Hartl, S. Oehler, and D.C. Lagoudas, Roundrobin SMA modeling article, in this volume, (2010)
[11] R. Delville, B. Malard, J. Pilch, P. Sittner, D. Schryvers, Int. J. of Plasticity, 27, (2010) 282 -297
[12] V. Novák, G.N. Dayananda, P. Šittner, F,M.Fernandes and K. K. Mahesh, Mat. Sci. Eng. A 481-482 (2008) 127-133
[13] L. Heller P. Sittner and J. Pilch, Impact of Heat Effects on Superelasticity, in proc. of ICOMAT 2008: Int'l Conference on Martensitic Transformations, Gregory B. Olson, David S. Lieberman, and Avadh B. Saxena, editors TMS, (2010) 445-452
[14] P. Blanc., C. Lexcellent, Materials Science and Engineering A, 378, 1-2 (2004) 465– 469.
[15] X. Gao, M. Huang, L.C. Brinson, Int. J. of Plasticity, 16, (2000) 1345– 1369.
[16] T.J.Lim, D.L. McDowell, J. Mech. Phys. Sol., 50 (2002) 651–676.
[17] E. Patoor, A. Eberhardt, M. Berveiller, J. Phys. IV, col. C1 6, (1996) 277–292.
[18] P. Thamburaja, L. Anand, Int. J. of Plasticity, 18, (2002) 1607– 617.
[19] A. Bhattacharyya, and G.J. Weng, J. Mech. Phys. Solides, 42, (1994) 1699– 1724.
[20] H. Andra, O. Hesebeck, L. Juhasz, J. of Applied Mathematics and Mechanics, 81, (2001) 329–330.
[21] F. Auricchio, R.L.Taylor, J. Lubliner, Comp. Meth. in Appl. Mech. and Eng., 146, 3-4, (1997) 281– 312.
[22] L.C. Brinson, J. of Intelligent Material Systems and Structures, 4, (1993) 229– 242.
[23] Y. Chemisky, A. Duval, E. Patoor, T. Ben Zineb, Mech. Mater., (2010) in print.
[24] M. Frost, P. Sedlak, M. Sippola and P. Sittner, Smart Mater. Struct. 19 (9), (2010), art. no. 094010
[25] S. Leclercq and C. Lexcellent, J. Mech. Phys. Sol., 44, (1996) 953–980.
[26] M. Panico, L.C. Brinson, J. Mech. Phys. Sol., 55, (2007) 2491–2511.
[27] B. Peultier, T. Ben Zineb and E. Patoor, Mech. Mater., 38 (2006) 510–524.
[28] P. Popov, D.C. Lagoudas, Int. J. of Plasticity, 23 (2007) 1679–1720.
[29] G. Rio, D. Favier, H. Desplats, J. Phys. IV, 5: C8, (1995) 215 – 220.
[30] L. Saint-Sulpice, S. Arbab Chirani. and S. Calloch, Mech. Mater., 41, (2009) 12– 26.
[31] K. Tanaka., Res. Mechanica, vol. 18 (1996) 251–263.
[32] F. Trochu, P. Terriault, Comp. Meth. Appl. Mech. Eng., 151 (1998) 545– 558.
[33] W. Zaki and Z. Moumni, J. Mech. Phys. Sol., 55 (2007) 2455–2490.
[34] J. Arghavani, F. Auricchio, R. Naghdabadi, A.Reali, S. Sohrabpour, Int. J. of Plasticity, 26 (2010) 976– 991.
[35] Y. Chemisky, A. Duval, B. Piotrowski, T. Ben Zineb, V.Tahiri, E. Patoor, Smart Mater. Struct, 18 (10), (2009) art. no. 104012.
[36] D.J. Hartl and D.C. Lagoudas, Smart Mater. Struct. 19 (1),(2010), art. no. 015020
[37] F. Jemal, T. Bouraoui, T. Ben Zineb , E. Patoor, and C. Bradai, Mech. Mater., 41 (2009) 849– 856.
[38] K. Taillard, P. Blanc, S. Calloch and C. Lexcellent, Mat. Sci. Eng. A 438-440 (2006) p. 436-440
[39] P. Šittner, P. Lukáš, V. Novák, M.R. Daymond, G.M. Swallowe, Mat. Sci. Eng. A 378, (2004) 97-104
[40] P. Šittner and V. Novák, Int. J. of Plasticity, 16 (2000) 1243-1268.